

JOURNAL OF MECHANICS OF CONTINUA AND MATHEMATICAL SCIENCES www.journalimcms.org



ISSN (Online): 2454 -7190 Vol.-20, No.-10, October (2025) pp 138-154 ISSN (Print) 0973-8975

ANALYSIS OF MAGNETOHYDRODYNAMIC NATURAL CONVECTION FLOW OF MICROPOLAR FLUID IN A SEMI-CIRCULAR ENCLOSURE FILLED

Gandrakota Kathyayani¹, Siddamsetti Maheswari² Gattu Venkata Ramudu³

^{1,2,3} Department of Applied Mathematics, Yogi Vemana University, Kadapa-516005 A. P, India.

Corresponding author: Gandrakota Kathyayani

Email: kathyagk@yvu.edu.in, maheswarisiddamsetti@gmail.com ramudu6594@gmail.com

https://doi.org/10.26782/jmcms.2025.10.00009

(Received: June 20, 2025; Revised: September 23, 2025; October 05, 2025)

Abstract

This study investigates the magnetohydrodynamic (MHD) natural convection flow of micropolar fluid in a semi-circular enclosure, incorporating the effects of thermal radiation. The analysis encompasses the interaction between buoyancy-driven flow, magnetic fields, radiative heat transfer, and the unique properties of micropolar fluids, which include microrotation and microstructure effects. The fundamental relations describing motion, thermal behavior, and rotational dynamics are established, incorporating the effects of the Lorentz force and radiative energy transfer. The Rosseland approximation is employed to model thermal radiation, and boundary conditions appropriate for a semi-circular geometry are applied. The governing relations are expressed in dimensionless form through characteristic parameters including the Rayleigh number (Ra), Prandtl number (Pr), Hartmann number (Ha), micropolar parameter (K), and radiation parameter (Rd). The modelled partial differential equations were carried out with a vorticity stream function algorithm to explore the influence of magnetic field strength, orientation, micropolar fluid properties, and radiative heat transfer on the flow and thermal characteristics. Results indicate significant alterations in flow patterns, temperature distribution, and microrotation behavior under varying magnetic field and radiative conditions. This comprehensive analysis provides insights into the complex dynamics of MHD natural convection in micropolar fluids with thermal radiation, with implications for advanced thermal management systems and materials processing applications.

Keywords: Semi-circular enclosure; Micropolar fluid; Stream function–vorticity formulation; Magneto-hydrodynamic; Finite differences.

I. Introduction

Micropolar fluids, first proposed by Eringen [VI], [VII], constitute a subclass of non-Newtonian fluids distinguished by intrinsic microstructural effects and an asymmetric stress tensor, thereby deviating from the conventional framework of the Navier-Stokes equations. This theory incorporates microrotation and additional velocity components, enabling more accurate modelling of flows in complex systems. Micropolar fluids are applicable in processes involving colloids, suspensions, metallic plate cooling, biological fluids, and rigid liquid crystals. Natural convection, driven by buoyancy from temperature-induced density variations, plays a crucial role in heat transport. When magnetic fields are applied (MHD effects), the flow behaviour becomes more intricate. Venkatadri et al. [XXVI] investigated such effects in enclosures, showing significant changes in flow and thermal profiles. Javed et al. [XI] extended the study to porous media, highlighting the combined impact of magnetism and micro polarity on convection structures. The role of thermal radiation in micropolar MHD flows has drawn attention. Perdikis et al. [XX] and Abd-El Aziz [II] demonstrated that radiation significantly modifies temperature and velocity fields. Hajatzadeh et al. [VIII] examined nanofluids under MHD convection and found enhanced heat transport due to magnetic and radiative effects. Similarly, Mahmoud [XV] and Bejawada et al. [IV] demonstrated that radiation may amplify or attenuate convection based on the characteristics of the fluid and boundary conditions. Investigations involving Casson fluids further advance the comprehension of intricate convective phenomena. Pop and Sheremet [XXI] analysed natural convection in square enclosures, observing that increasing the Casson parameter improves heat transfer. Devi et al. [V] explored Casson viscoplastic fluids, revealing similar enhancements under varied Rayleigh and radiation parameters. Ismail et al. [III] evaluated tri-hybrid Casson nanofluids in different cavity shapes, concluding that thermal radiation, porosity, and Casson parameters stabilize and enhance thermal performance.

The study of non-Newtonian fluids continues to expand. Venkatadri et al. [XXVIII] applied the Buongiorno model to analyze magnetic nanofluid flow in a 2D porous fuel cell. Using a finite difference method (FDM) and vorticity–stream function (VSF) approach, they showed that stronger magnetic fields (higher Hartmann number) suppress local Nusselt numbers while Brownian motion increases both Nusselt and Sherwood numbers at the cold walls. Various cavity shapes, such as square, circular, and alphabet-based geometries (L, T, H, C, V, W, M, I) have been explored to improve thermal transport efficiency [X, XXIV, XVI, XVIII, XXV, XVII, I]. Such geometrical configurations affect convection patterns and heat transfer rates according to the fluid characteristics and flow regime. Examining micropolar fluid motion within a semi-circular enclosure is especially significant owing to its practical applications in thermal insulation, electronic cooling, and heat exchanger design. In such systems, the interaction between the Lorentz force and micropolar fluid properties can significantly enhance heat transfer. Environmental applications like pollutant transport and subsurface flow also benefit from understanding such convective behaviors.

However, limited studies address the combined effect of thermal radiation and magnetic fields in micropolar fluid convection, particularly in non-rectangular

domains. Therefore, the current computational work focuses on natural convection of micropolar fluid in a semi-circular heated enclosure under a transverse uniform magnetic field. The objective is to analyze the resulting fluid dynamics and heat transfer characteristics, contributing to improved design in thermal management systems.

II. Mathematical Formulation

A two-dimensional computational semi-circular domain occupied by micropolar fluid and a magnetic field (B₀) is present in the y-direction. This is depicted in **Figure 1.** The applied magnetic field induces a Lorentz body force acting perpendicularly, while the semi-circular enclosure is subjected to uniform heating along the bottom wall and maintained at a constant cold temperature along the curved wall. To account for density variations in the buoyancy term, the Boussinesq approximation is employed. The electroconductive micropolar fluid is assumed to possess constant thermophysical properties, with viscous dissipation, chemical reactions, and Joule heating effects neglected. Under these assumptions, the dimensional governing equations for the conservation of momentum, mass, and energy can be formulated, following the framework outlined in [XIV, XXIII], as:

Continuity Equation:

$$\nabla \cdot \boldsymbol{u} = 0 \tag{1}$$

Momentum Equation:

$$\rho \left(\frac{\partial \boldsymbol{u}}{\partial t} + (\boldsymbol{u} \cdot \nabla) \boldsymbol{u} \right) = -\nabla P + \mu \nabla^2 \boldsymbol{u} + \kappa \nabla^2 N + \rho \boldsymbol{g} \beta (T - T_c) + \boldsymbol{J} \times \boldsymbol{B}$$
 (2)

P – Pressure, μ - Dynamic viscosity, κ - coupling coefficient, N - microrotation vector, g - gravitational acceleration, β - thermal expansion coefficient, T - temperature, T_c - reference temperature, T_c - current density, T_c - magnetic field.

$$J = \sigma(E + u \times B)
\nabla \times B = \mu_0 J$$

Angular Momentum Equation:

$$\rho j \left(\frac{\partial N}{\partial t} + (\boldsymbol{u} \cdot \nabla) \boldsymbol{N} \right) = \gamma \nabla^2 N - 2\kappa \boldsymbol{N} + \kappa \nabla \times \boldsymbol{u}$$
 (3)

 γ - spin gradient, j - gyration parameter, κ - signifies vortex viscosity.

Energy Equation:

$$\rho c_p \left(\frac{\partial T}{\partial t} + (\boldsymbol{u} \cdot \nabla) T \right) = k \nabla^2 T - \nabla q_r \tag{4}$$

 c_p - specific heat capacity, q_r - radiative heat flux, k - thermal conductivity.

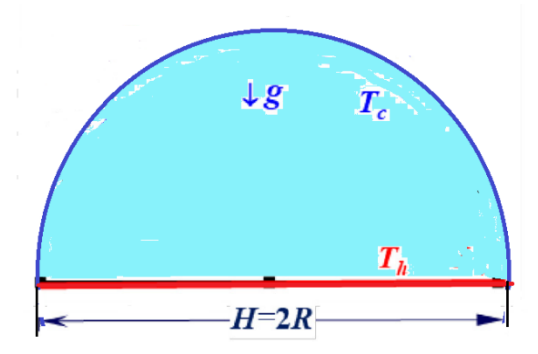


Fig. 1. Computational Flow Geometry

The Cartesian form of the above modelling equations is as follows:

$$\frac{\partial u}{\partial x} + \frac{\partial v}{\partial y} = 0 \tag{5}$$

$$\rho\left(\frac{\partial u}{\partial t} + u\frac{\partial u}{\partial x} + v\frac{\partial u}{\partial y}\right) = -\frac{\partial p}{\partial x} + (\mu + k)\left(\frac{\partial^2 u}{\partial x^2} + \frac{\partial^2 u}{\partial y^2}\right) + k\frac{\partial N^*}{\partial y}$$
(6)

$$\rho\left(\frac{\partial v}{\partial t} + u\frac{\partial v}{\partial x} + v\frac{\partial v}{\partial y}\right) = -\frac{\partial p}{\partial y} + (\mu + k)\left(\frac{\partial^2 v}{\partial x^2} + \frac{\partial^2 v}{\partial y^2}\right) - \sigma B_0^2 v - k\frac{\partial N^*}{\partial x} + \rho g(T - T_c)$$
 (7)

$$\rho j \left(u \frac{\partial N^*}{\partial x} + v \frac{\partial N^*}{\partial y} + \frac{\partial N^*}{\partial t} \right) + 2kN^* = k \left(\frac{\partial v}{\partial x} - \frac{\partial u}{\partial y} \right) + \gamma \left(\frac{\partial^2 N^*}{\partial x^2} + \frac{\partial^2 N^*}{\partial y^2} \right) \tag{8}$$

$$\frac{\partial T}{\partial t} + u \frac{\partial T}{\partial x} + v \frac{\partial T}{\partial y} = \alpha_f \left(\frac{\partial^2 T}{\partial x^2} + \frac{\partial^2 T}{\partial y^2} \right) - \frac{1}{(\rho C_p)_f} \left(\frac{\partial q_x}{\partial \bar{x}} + \frac{\partial q_y}{\partial \bar{y}} \right)$$
(9)

where
$$(q_{rx}, q_{ry}) = \left(-\frac{4\sigma}{3k^*} \frac{\partial T^4}{\partial x}, -\frac{4\sigma}{3k^*} \frac{\partial T^4}{\partial y}\right)$$

The prescribed initial boundary conditions of the present semi-circular enclosure are as follows:

At t=0 with for
$$0 \le x, y \le L : 0 = u = T = v = N^*$$

 $T = T_c, N^* = n \frac{\partial v}{\partial n}$ at the curved boundary
 $T = T_h, N^* = n \frac{\partial v}{\partial x}$ at the bottom wall

All boundaries,
$$0 = u = v$$
 (10)

The equations (5) - (9) can be written in dimensionless form with the help of quantities defined below:

$$\tau = \frac{t\alpha}{L^2}, X = \frac{x}{L}, Y = \frac{y}{L}, U = \frac{uL}{\alpha}, V = \frac{vL}{\alpha}, \theta = \frac{T - T_c}{T_h - T_c}, N = \frac{N^* L^2}{\alpha} P = \frac{L^2 p}{\alpha^2 \rho_f}$$
(11)

The non-dimensional form of the interpreted governing equations is:

$$\frac{\partial U}{\partial x} = -\frac{\partial V}{\partial Y} \tag{12}$$

$$\frac{\partial U}{\partial X} = -\frac{\partial V}{\partial Y}$$

$$\frac{\partial U}{\partial \tau} + \frac{\partial P}{\partial X} = (1 + K) Pr \left(\frac{\partial^2 U}{\partial X^2} + \frac{\partial^2 U}{\partial Y^2} \right) - \left(U \frac{\partial U}{\partial X} + V \frac{\partial U}{\partial Y} \right) + K Pr \frac{\partial N}{\partial Y}$$
(12)

$$\frac{\partial V}{\partial \tau} + \frac{\partial P}{\partial Y} = (1 + K) \Pr\left(\frac{\partial^{2} V}{\partial x^{2}} + \frac{\partial^{2} V}{\partial Y^{2}}\right) - \left(U\frac{\partial V}{\partial x} + V\frac{\partial V}{\partial Y}\right) - K\Pr\left(\frac{\partial N}{\partial x} - H\alpha^{2}PrV + R\alpha Pr\theta\right) (14)$$

$$\frac{\partial N}{\partial \tau} + U\frac{\partial N}{\partial x} + V\frac{\partial N}{\partial Y} = \left(1 + \frac{K}{2}\right) Pr\left(\frac{\partial^{2} N}{\partial x^{2}} + \frac{\partial^{2} N}{\partial Y^{2}}\right) - 2KN Pr + K Pr\left(\frac{\partial V}{\partial x} - \frac{\partial U}{\partial Y}\right)$$

$$\frac{\partial \theta}{\partial \tau} + U\frac{\partial \theta}{\partial x} + V\frac{\partial \theta}{\partial Y} = \left(1 + \frac{4}{3}Rd\right) \left(\frac{\partial^{2} \theta}{\partial x^{2}} + \frac{\partial^{2} \theta}{\partial Y^{2}}\right)$$
(15)

The boundary conditions applied to the computational domain are specified as follows:

On the enclosure walls (base and curved walls): U = 0, V = 0

Base wall:
$$\theta = 1, N = n \frac{\partial v}{\partial x}$$
.

Curved wall:
$$\theta = 0, N = -n \frac{\partial U}{\partial Y}$$
. (17)

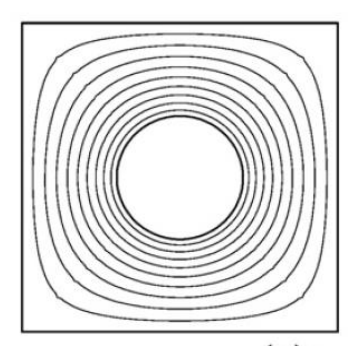
The heat transfer rate (Local Nusselt number) along the base hot wall is measured the follows:

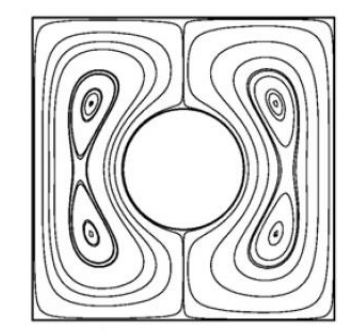
$$Nu = \frac{\partial \theta}{\partial y} \tag{18}$$

The representative measure of heat transfer, expressed through the average Nusselt number, can be written as

$$Nu_{avg} = \int_0^1 \frac{\partial \theta}{\partial Y} dX$$
 (19)

It should be emphasized that all reported computations were performed with n=0, i.e., under the strong anchoring (no-spin) boundary condition. This ensures that microrotation vanishes identically at the solid walls, consistent with rigid-wall assumptions in micropolar theory. While alternative treatments (e.g., weak anchoring or spin-velocity coupling) are possible, the strong anchoring case was selected here as it is the most widely used and provides a baseline for comparison with published results.





Hussain et al., [IX] Results

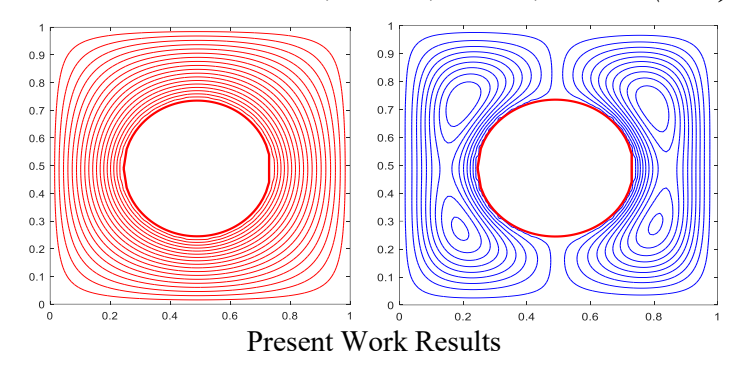


Fig. 2. Comparative visualization of temperature distributions (isotherms) and flow structures (streamlines).

III. Numerical methodology and code validation

The pressure-based governing momentum equations are highly complex; therefore, their solution is obtained as follows:

$$U = \frac{\partial \psi}{\partial Y}, V = -\frac{\partial \psi}{\partial X} \tag{20}$$

$$\left(\frac{\partial^2 \psi}{\partial X^2} + \frac{\partial^2 \psi}{\partial Y^2}\right) = -\omega \tag{21}$$

$$\frac{\partial \omega}{\partial \tau} + U \frac{\partial \omega}{\partial X} + V \frac{\partial \omega}{\partial Y} = (1 + K) Pr \left(\frac{\partial^2 \omega}{\partial X^2} + \frac{\partial^2 \omega}{\partial Y^2} \right)$$

$$-K Pr\left(\frac{\partial^{2} N}{\partial x^{2}} + \frac{\partial^{2} N}{\partial y^{2}}\right) - Ha^{2} Pr \frac{\partial V}{\partial x} + Ra. Pr \frac{\partial \theta}{\partial x}$$
 (22)

The vorticity stream function approach was used to solve the modelled partial differential equations numerically. Collocated grid is the advancement of the computational grid system. A second-order finite difference approximation is used to discretise the equations under control. The iterative Linear Successive Over-Relaxation (LSOR) approach is employed to solve the discretised algebraic equations. The numerical computation was proceeded until they met the convergent criterion of each variable (i.e., ω, ψ, θ), which was $\sum_{i,j} |\Omega_{i,j}^{k+1} - \Omega_{i,j}^k| < 10^{-8}$, here k refers to the iteration levels. The readers found complete details of the vorticity stream function approach in Ref. [XXII, XXVII, XXX, XXIX, XII]. Computational stability was maintained by adhering to standard Fourier and Courant–Friedrichs–Lewy (CFL) criteria. For the explicit parts of the scheme, CFL numbers were kept below unity (CFL ≤ 1), while the Fourier number for thermal diffusion satisfied Fo ≤ 0.5 . These conditions ensured stability across all simulations

It is important to emphasize that the numerical scheme validation for the research data of the closed study. In a study conducted by Hussain et al. [IX], Figure 2 illustrates the findings of natural convection within an air-filled square enclosure at $Ra = 10^3$. In contrast, the present study rigorously examined with the Finite Difference Method (FDM) and then compared the results to those reported by Hussain et al. [IX]. Studied the flow driven by buoyancy in a square chamber using a heated circular cylinder, and then compared with the previous research conducted by Kim et al. [XIII, XIX]. Hence,

the present numerical simulation compares and verifies both the performance is presented in **Table 1**. Here, the current numerical scheme results give good agreement with the work of Kim et al. [XIII] and Kim et. al. [XIX].

To ensure numerical accuracy, a systematic grid refinement study was performed. Three progressively refined meshes were considered: 80×40 (coarse), 120×60 (medium), and 160×80 (fine). The average Nusselt number along the heated bottom wall was monitored for each case. The variation in Nu between the medium and fine grids was found to be less than 2%, demonstrating grid-independent solutions. Table 1 summarizes the Nu values for the different grids, while Figure 2 shows the comparison of isotherms and streamlines for the medium and fine meshes, which are nearly identical.

Ra	Nu	Error Percentage			
	Kim et. al. [25]	Kim et. al. [26]	3. Present study	1&3	2&3
103	5.02	5.093	5.039	1.06	1.06
104	5.113	5.108	5.131	0.35	0.35
105	7.75	7.767	7.807	0.73	0.512
106	14.2	14.11	14.13	0.49	0.1415

Table 1: Validation of Nu with the benchmark results.

IV. Results and Discussion

The effects of key emerging parameters, including the magnetic number ($0 \le \text{Ha} \le 30$), vortex viscosity parameter ($1 \le K \le 5$), Rayleigh number ($10^3 \le \text{Ra} \le 10^6$), and thermal radiation parameter ($0 \le \text{Rd} \le 5$), on hydromagnetic micropolar fluid flow and heat transfer in a semi-circular enclosure are examined in this section. Contour plots are provided to illustrate the influence of these parameters.

Figure 3 depicts the effect of thermal buoyancy (Ra) on flow structures, temperature fields (isotherms), and microrotation contours within the semi-circular enclosure for Rd = 1, K = 1, Ha = 2, and Pr = 6.2, where Ra increases from 10^3 at the bottom to 10^6 at the top. As Ra increases, the flow patterns (first column) transition from weak, symmetric circulations to strong, complex convective currents. The temperature distribution (second column) shifts from nearly uniform, conduction-dominated isotherms to highly distorted, convection-dominated patterns. Similarly, the microrotation fields (third column) evolve from minimal variations to intricate and dynamic contours, reflecting stronger interactions between the fluid flow and microrotation. These changes highlight the enhanced convective heat transfer and fluid mixing capabilities at higher Rayleigh numbers within the enclosure.

Figure 4 illustrates the influence of the vortex-viscosity parameter K on streamlines, isotherms, and iso-microrotation in a semi-circular enclosure with Rd = 1, Ra= 10^5 , Ha = 2, and Pr = 6.2, where K increases from 1 at the bottom to 5 at the top. As K increases,

the flow intensity decreases. The streamlines (first column) show that at K=1, the convective currents are vigorous and display complex, well-defined circulation patterns. As K increases to 3, 4, and finally 5, the intensity of these circulations diminishes, and the flow patterns become simpler and less pronounced, indicating weaker convective activity. The temperature distribution (second column) also shows a decrease in intensity with increasing K. At K=1, the isotherms are highly distorted, reflecting strong convective heat transfer and significant temperature gradients. As K increases, the isotherms become more uniform and parallel, indicating a reduction in convective effects and a dominance of conductive heat transfer. Similarly, the microrotation fields (third column) exhibit a decrease in complexity and intensity as K increases. At K=1, the iso-microrotation lines are complex and dynamic, showing significant microrotation activity. As K increases to 3, 4, and 5, these lines become more uniform and less varied, reflecting diminished microrotation effects and interactions with the fluid flow. Overall, as the vortex-viscosity parameter K increases, both the flow intensity and temperature gradients within the semi-circular enclosure decrease, leading to simpler, less dynamic fluid motion, temperature distribution, and microrotation fields

Figure 5 illustrates the influence of the magnetic field on streamlines, thermal distribution, and iso-microrotation for a semicircular cavity with parameters Rd = 1, $Ra=10^5$, K=1, and Pr=6.2. Each row represents different Ha values: 0, 10, 20, and 30 (from top to bottom), while the columns depict streamlines, isotherms, and isomicrorotation (from left to right). As Ha increases, the Lorentz force, which opposes the motion of conducting fluids in the presence of a magnetic field, becomes more significant. This force damps the fluid motion, leading to more streamlined and less complex flow patterns, with fewer vortices at higher Ha values. The isotherms transition from wavy to more horizontal, indicating a suppression of buoyancy-driven convection and a dominance of conductive heat transfer as the magnetic field strength increases. The iso-microrotation contours show a decrease in complexity and more uniform distribution, reflecting the stabilizing influence of the magnetic field on rotational motion within the fluid. Overall, increasing Ha stabilizes the flow, reduces the complexity of temperature and microrotation distributions, and suppresses convective effects, consistent with the physical understanding that a stronger magnetic field enhances flow stability and reduces turbulence through the damping effect of the Lorentz force.

Figure 6 shows the local Nusselt number (Nu) distribution along the bottom wall of a semicircular enclosure for various Rayleigh number values (Ra = 10^3 , 10^4 , 10^5 , 10^6) with other fixed parameters, Rd = K=1, Ha = 2. As Ra increases, the Nu distribution's amplitude rises, indicating stronger buoyancy-driven convection. For Ra = 10^3 , the distribution is relatively smooth with lower values, suggesting weak convection. As Ra increases to 10^4 and 10^5 , the amplitude and the peaks and valleys become more pronounced, reflecting enhanced convective effects. At Ra = 10^6 , the highest amplitude and significant variations in Nu indicate very strong convective heat transfer. Maximum and minimum Nu values are observed near the edges, while the central region shows lower values for all Ra cases. This trend emphasizes the growing dominance of buoyancy forces and the shift from conduction-controlled to convection-controlled heat transfer as Ra increases.

Figure 7 displays the local Nusselt number (Nu) distribution along the hot bottom wall of a semicircular cavity for different Hartmann numbers (Ha = 0, 10, 20, 30) with parameters Rd = K=1, $Ra = 10^6$. As Ha increases, the Nu distribution's amplitude decreases, indicating a reduction in convective heat transfer and a shift towards conductive heat transfer. For Ha = 0, the distribution shows higher peaks and valleys, reflecting strong convection. As Ha increases to 10 and 20, the peaks and valleys moderate, and at Ha = 30, the distribution becomes the smoothest, indicating the significant damping effect of the Lorentz force on fluid motion. The maximum and minimum Nu values are near the edges, with the central region showing the lowest values for all Ha cases. This trend highlights the stabilizing influence of the magnetic field, reducing buoyancy-driven convection and enhancing flow stability.

Figure 8 presents the distribution of the local Nusselt number (Nu) along the heated bottom wall (X-axis) for different values of the radiation parameter (Rd), with the magnetic field parameter fixed at Ha = 2 and the vortex viscosity parameter at K = 1. The X-axis extends from 0 to 1, while the Y-axis spans 0 to 180. Four curves correspond to Rd = 0 (blue), Rd = 1 (black), Rd = 3 (green), and Rd = 5 (red). The results show that the Nusselt number, which characterizes the ratio of convective to conductive heat transfer, decreases from both ends toward the mid-section for all Rd values, signifying enhanced heat transfer near the enclosure walls and reduced transfer at the center. As Rd increases, the local Nusselt number also increases, reflecting the enhanced radiative heat transfer contribution. This trend shows that radiation significantly boosts the overall heat transfer, especially at higher Rd values. The magnetic field (Ha=2) and thermal conductivity ratio (K=1) remain constant, suggesting that the observed variations in heat transfer are primarily due to changes in the radiative parameter (Rd). The Rd=0 curve has the lowest Nusselt values, while the Rd=5 curve has the highest, demonstrating the substantial impact of radiation on local heat transfer along the wall.

V. Conclusion

Using the vorticity stream function approach, two-dimensional magnetized micropolar fluid flow of natural convection in a semi-circular enclosure has been numerically analyzed. The present analysis investigates the effects of thermal radiation, Lorentz forces, and the vortex viscosity parameter using the finite difference method. The semi-circular enclosure is assumed to contain an electrically conducting micropolar fluid in thermal equilibrium. The governing nonlinear partial differential equations of momentum, energy, and mass conservation are solved subject to the prescribed wall boundary conditions for a conventional micropolar fluid. The numerical computations yield several significant findings, which are summarized below:

- Increasing the vortex-viscosity parameter K results in a weakening of the convective flow. This is evidenced by the elongation and reduced intensity of the streamlines, the more uniform distribution of isotherms, and the increased complexity in iso-microrotation contours.
- The two symmetric circulations are developed in all the cases except the high (or strong) buoyancy force $Ra = 10^6$.

- There is a noticeable upward trend in the local Nusselt number with increasing Rd values, indicating a stronger heat transfer effect with higher Rd.
- For all Ra values, the Nusselt number starts high at X=0, dips towards the middle, and then rises again towards X=1. The significant dips and peaks for higher Ra suggest that the system is more sensitive to changes in X for higher Rayleigh numbers.
- Increasing Ha boosts *Nu* on the hot wall, showing that stronger magnetic fields suppress convective currents and reduce heat transfer efficiency.

Disclosure of Competing Interests

The authors state that none of the work described in this study could have been influenced by any known competing financial interests or personal relationships.

Statement about conflicts of interest

Any potential conflicts of interest were not disclosed by the writers.

Statement of Data Availability

The text has no associated data.

Declaration of Funding

No specific grant from a public, private, or nonprofit funding organisation was obtained for this study.

Nomenclature:

Symbol	Description	Symbol	Description	
B_0	Magnetic field	p	Pressure	
C_p	Specific heat	t	Time	
На	Hartmann number	T	Temperature	
g	gravitational acceleration	N^*	Dimensionless micro rotation angular velocity	
Pr	Prandtl number	(U, V)	Dimensionless velocity component in X, Y-direction	
N	Dimensional micro rotation angular velocity	(x,y)	Cartesian coordinates in horizontal and vertical directions	
K	Vortex viscosity parameter	Rd	Thermal radiation	
L	Length of the enclosure	Н	Height of the enclosure	
Ra	Rayleigh number	Greek lett	ek letters	
K	Dimensionless vortex viscosity	μ	Dynamic viscosity	
(X, Y)	Dimensionless coordinate in horizontal and vertical directions	ρ	Fluid density	
(u,v)	Dimensional component of fluid velocity in x, y-direction	γ	Spin-gradient viscosity	
T_c	Temperature at cold wall	τ	Non-dimensional time	
T_h	Temperature at hot wall	α	Thermal diffusivity	
Nu	Local Nusselt number	θ	Non-dimensional temperature	

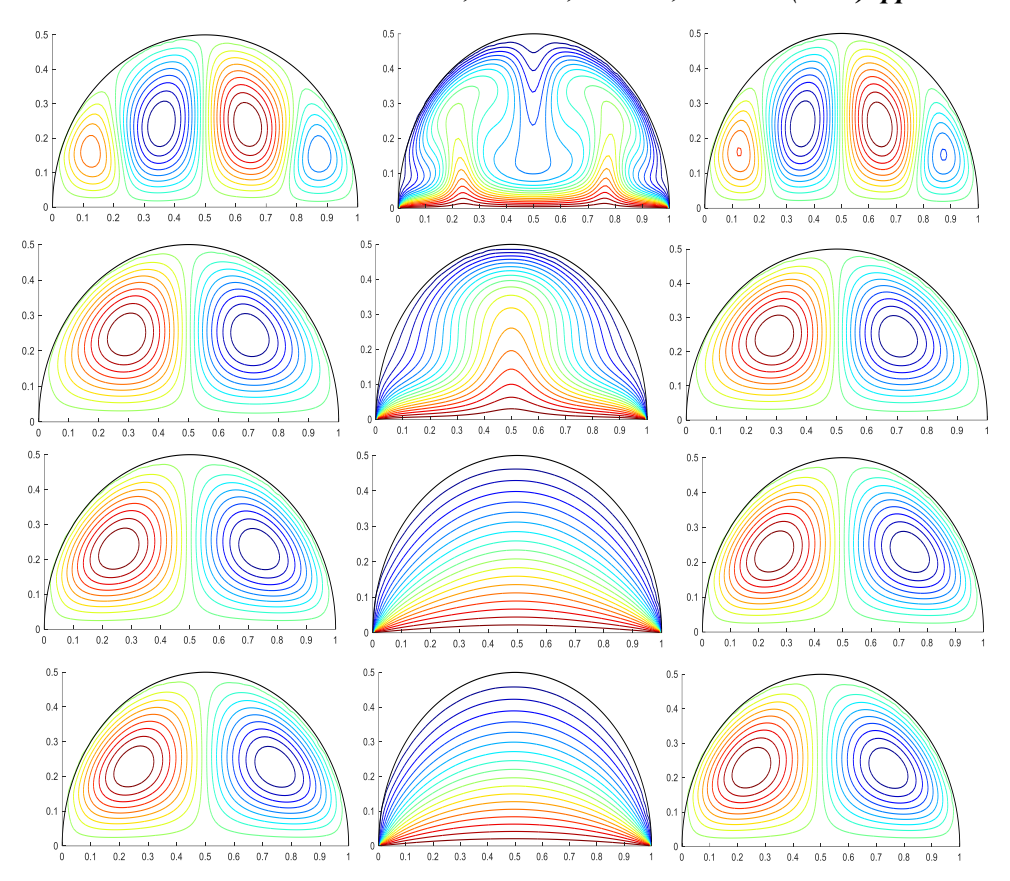
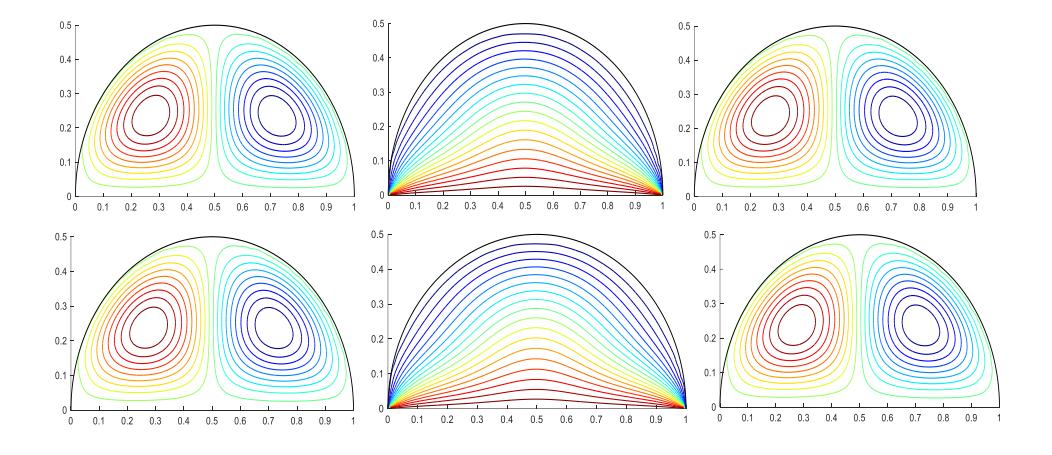


Fig. 3. The influence of the Ra on streamlines, isotherms, and iso-microrotation with Rd =1, K=1, Ha = 2, and Pr = 6.2.



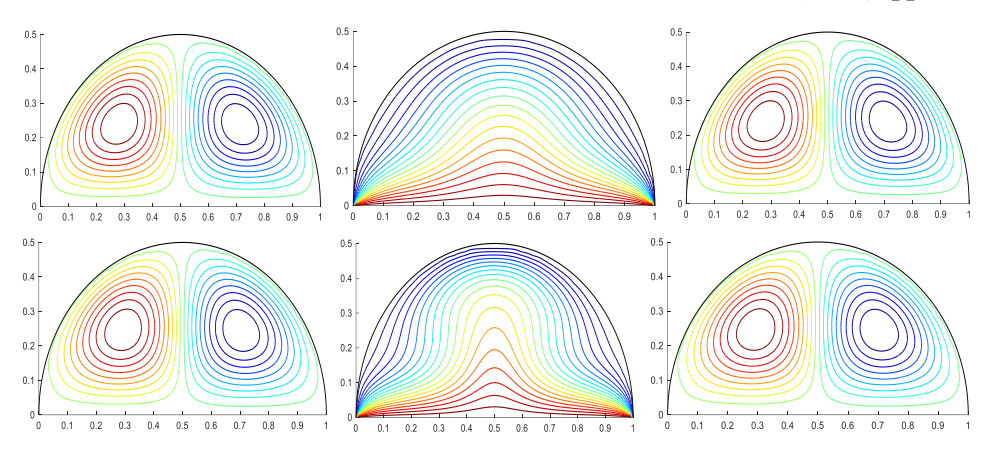


Fig. 4. The influence of the vortex-viscosity parameter K=1, 3, 4, and 5 (from bottom to top) on streamlines, isotherms, and iso-microrotation with Rd=1, $Ra=10^5$, Ha=2, and Pr=6.2.

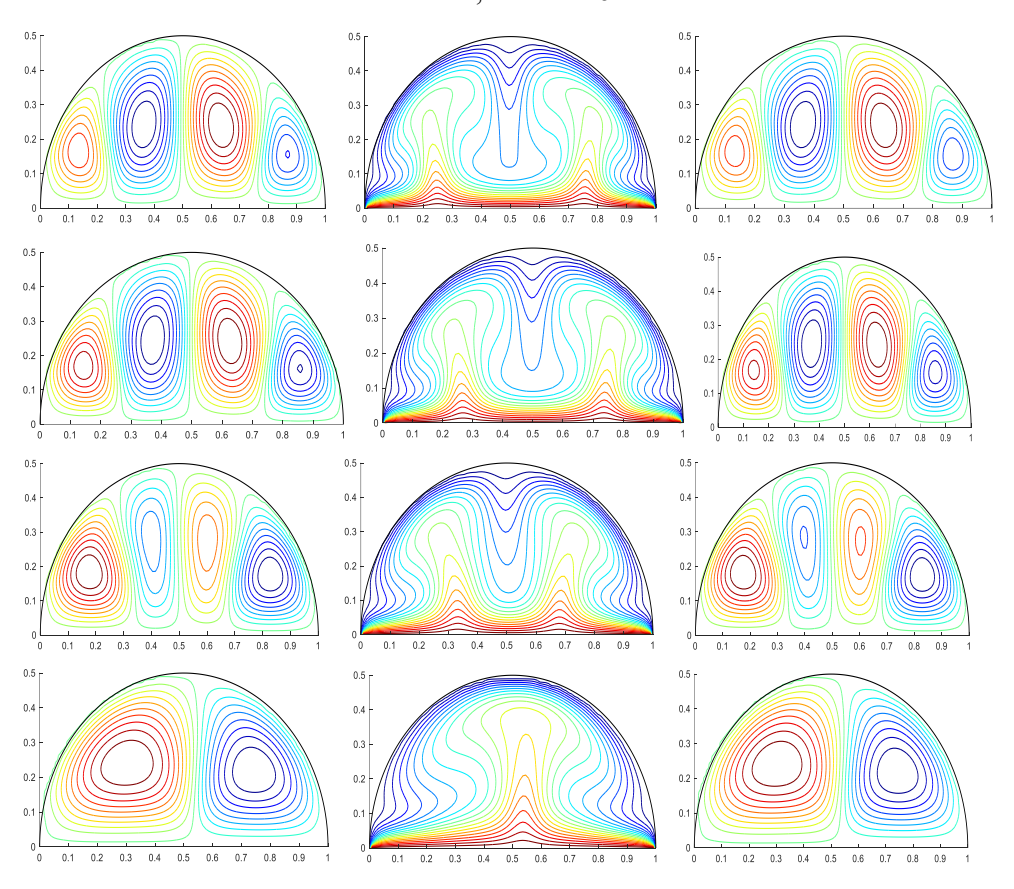


Fig. 5. The influence of the Ha = 30, 20, 10, and 0 (from bottom to top) on streamlines, isotherms, and iso-microrotation with Rd =1, Ra= 10^5 , K = 1, and Pr = 6.2.

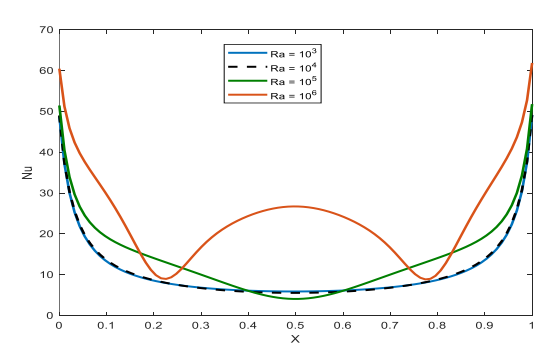


Fig. 6. Local Nusselt number distribution for various Ra values at Rd = 1, K = 1, and Ha = 2 along the heated bottom wall.

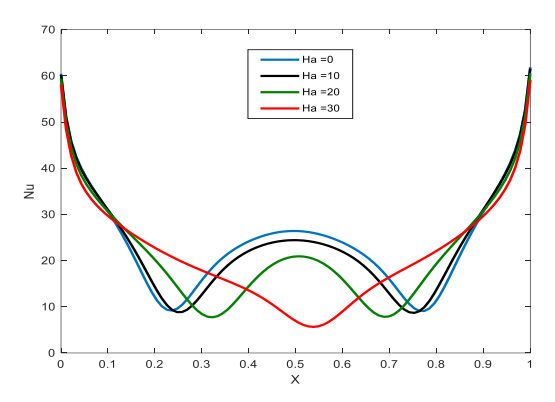


Fig. 7. Distribution of the local Nusselt number along the heated bottom wall for various Ha values at Rd = 1, K = 1, and $Ra = 10^6$.

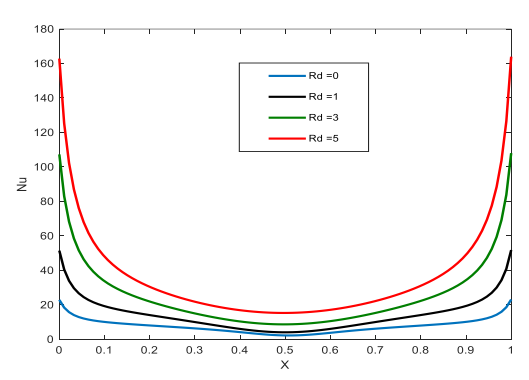


Fig. 8. Distribution of the local Nusselt number along the heated bottom wall for various Rd values at K = 1 and Ha = 2.

Conflict of Interest

The authors declare that there is no conflict of interest this paper.

References

- I. Ababaei, A., M. Abbaszadeh, A. Arefmanesh, and A. J. Chamkha. "Numerical Simulation of Double-Diffusive Mixed Convection and Entropy Generation in a Lid-Driven Trapezoidal Enclosure with a Heat Source." *Numerical Heat Transfer, Part A: Applications*, vol. 73, no. 10, 2018, pp. 702–720. 10.1080/10407782.2018.1459139.
- II. Abd-El Aziz, M. "Thermal Radiation Effects on Magnetohydrodynamic Mixed Convection Flow of a Micropolar Fluid Past a Continuously Moving Semi-Infinite Plate for High Temperature Differences." *Acta Mechanica*, vol. 187, 2006, pp. 113–127. 10.1007/s00707-006-0377-9.
- III. Bhadauria, B. S., A. Kumar, S. K. Rawat, and M. Yaseen. "Thermal Instability of Tri-Hybrid Casson Nanofluid with Thermal Radiation Saturated Porous Medium in Different Enclosures." *Chinese Journal of Physics*, vol. 87, 2024, pp. 710–727. 10.1016/j.cjph.2023.12.032.
- IV. Bejawada, S. G., and M. M. Nandeppanavar. "Effect of Thermal Radiation on Magnetohydrodynamics Heat Transfer Micropolar Fluid Flow over a Vertical Moving Porous Plate." *Experimental and Computational Multiphase Flow*, vol. 5, 2023, pp. 149–158. 10.1007/s42757-021-0131-5.
- V. Devi, T. S., C. V. Lakshmi, K. Venkatadri, V. R. Prasad, O. A. Bég, and M. S. Reddy. "Simulation of Unsteady Natural Convection Flow of a Casson Viscoplastic Fluid in a Square Enclosure Utilizing a MAC Algorithm." *Heat Transfer*, vol. 49, no. 4, 2020, pp. 1769–1787. 10.1002/htj.21690.
- VI. Eringen, A. C. "Theory of Micropolar Fluids." *Journal of Mathematics and Mechanics*, vol. 16, 1966, pp. 1–18.
- VII. Eringen, A. C. "Theory of Thermomicrofluids." *Journal of Mathematical Analysis and Applications*, vol. 38, 1972, pp. 480–496. 10.1016/0022-247X(72)90106-0.
- VIII. Hajatzadeh Pordanjani, A., S. Aghakhani, A. Karimipour, et al. "Investigation of Free Convection Heat Transfer and Entropy Generation of Nanofluid Flow Inside a Cavity Affected by Magnetic Field and Thermal Radiation." *Journal of Thermal Analysis and Calorimetry*, vol. 137, 2019, pp. 997–1019. 10.1007/s10973-018-7982-4.
- IX. Hussain, S. H., and A. K. Hussein. "Numerical Investigation of Natural Convection Phenomena in a Uniformly Heated Circular Cylinder Immersed in Square Enclosure Filled with Air at Different Vertical Locations." *International Communications in Heat and Mass Transfer*, vol. 37, no. 8, 2010, pp. 1115–1126. 10.1016/j.icheatmasstransfer.2010.05.016.

- X. Hussam, W. K., K. Khanafer, H. J. Salem, and G. J. Sheard. "Natural Convection Heat Transfer Utilizing Nanofluid in a Cavity with a Periodic Side-Wall Temperature in the Presence of a Magnetic Field." *International Communications in Heat and Mass Transfer*, vol. 104, 2019, pp. 127–135. 10.1016/j.icheatmasstransfer.2019.02.018.
- XI. Javed, T., Z. Mehmood, and M. A. Siddiqui. "Mixed Convection in a Triangular Cavity Permeated with Micropolar Nanofluid-Saturated Porous Medium under the Impact of MHD." *Journal of the Brazilian Society of Mechanical Sciences and Engineering*, vol. 39, 2017, pp. 3897–3909. 10.1007/s40430-017-0850-5.
- XII. Kathyayani, G., and Venkata Ramudu G. "MHD Double-Diffusive Convection of Casson Fluid in a Triangular Enclosure with Thermal Radiation and Chemical Reactions." *Multiscale and Multidisciplinary Modeling, Experiments and Design*, vol. 8, 2025, p. 289. 10.1007/s41939-025-00874-4.
- XIII. Kim, B. S., D. S. Lee, M. Y. Ha, and H. S. Yoon. "A Numerical Study of Natural Convection in a Square Enclosure with a Circular Cylinder at Different Vertical Locations." *International Journal of Heat and Mass Transfer*, vol. 51, no. 7, 2008, pp. 1888–1906. 10.1016/j.ijheatmasstransfer.2007.06.033.
- XIV. Lee, J. M., M. Y. Ha, and H. S. Yoon. "Natural Convection in a Square Enclosure with a Circular Cylinder at Different Horizontal and Diagonal Locations." *International Journal of Heat and Mass Transfer*, vol. 53, no. 25-26, 2010, pp. 5905–5919. 10.1016/j.ijheatmasstransfer.2010.07.043.
- XV. Mahmoud, M. A. "Thermal Radiation Effects on MHD Flow of a Micropolar Fluid over a Stretching Surface with Variable Thermal Conductivity." *Physica A: Statistical Mechanics and Its Applications*, vol. 375, no. 2, 2007, pp. 401–410. 10.1016/j.physa.2006.09.010.
- XVI. Mojumder, S., S. Saha, S. Saha, and M. A. H. Mamun. "Effect of Magnetic Field on Natural Convection in a C-Shaped Cavity Filled with Ferrofluid." *Procedia Engineering*, vol. 105, 2015, pp. 96–104. 10.1016/j.proeng.2015.05.012.
- XVII. Nia, S. N., F. Rabiei, M. M. Rashidi, and T. M. Kwang. "Lattice Boltzmann Simulation of Natural Convection Heat Transfer of a Nanofluid in a L-Shape Enclosure with a Baffle." *Results in Physics*, vol. 19, 2020, p. 103413. 10.1016/j.rinp.2020.103413.
- XVIII. Parvin, S., and A. J. Chamkha. "An Analysis on Free Convection Flow, Heat Transfer and Entropy Generation in an Odd-Shaped Cavity Filled with Nanofluid." *International Communications in Heat and Mass Transfer*, vol. 54, 2014, pp. 8–17. 10.1016/j.icheatmasstransfer.2014.02.031.
- XIX. Park, J., M. Kim, G. S. Mun, et al. "Natural Convection in a Square Enclosure with a Circular Cylinder with Adiabatic Side Walls According to Bottom Wall Temperature Variation." *Journal of Mechanical Science and Technology*, vol. 32,pp. 3201–3211. 10.1007/s12206-018-0623-9.

- XX. Perdikis, C., and A. Raptis. "Heat Transfer of a Micropolar Fluid by the Presence of Radiation." *Heat and Mass Transfer*, vol. 31, 1996, pp. 381–382. 10.1007/BF02172582.
- XXI. Pop, I., and M. Sheremet. "Free Convection in a Square Cavity Filled with a Casson Fluid under the Effects of Thermal Radiation and Viscous Dissipation." *International Journal of Numerical Methods for Heat & Fluid Flow*, vol. 27, no. 10, 2017, pp. 2318–2332. 10.1108/HFF-09-2016-0352.
- XXII. Raja Rajeswari, V., K. Venkatadri, and V. Ramachandra Prasad. "Nanoparticle Shape Factor Impact on Double Diffusive Convection of Cu-Water Nanofluid in Trapezoidal Porous Enclosures: A Numerical Study." *Numerical Heat Transfer, Part A: Applications*, 2024, pp. 1–20. 10.1080/10407782.2024.2380814.
- XXIII. Singhal, R., S. Dutta, and J. C. Kalita. "Comprehensive Study of Forced Convection over a Heated Elliptical Cylinder with Varying Angle of Incidences to Uniform Free Stream." *International Journal of Thermal Sciences*, vol. 194, 2023, p. 108588. 10.1016/j.ijthermalsci.2023.108588.
- XXIV. Varol, Y., H. F. Oztop, and T. Yilmaz. "Natural Convection in Triangular Enclosures with Protruding Isothermal Heater." *International Journal of Heat and Mass Transfer*, vol. 50, no. 13–14, 2007, pp. 2451–2462. 10.1016/j.ijheatmasstransfer.2006.12.027.
- XXV. Venkatadri, K., O. A. Bég, P. Rajarajeswari, and V. R. Prasad. "Numerical Simulation of Thermal Radiation Influence on Natural Convection in a Trapezoidal Enclosure: Heat Flow Visualization through Energy Flux Vectors." *International Journal of Mechanical Sciences*, vol. 171, 2020, p. 105391. 10.1016/j.ijmecsci.2019.105391.
- XXVI. Venkatadri, K., V. Ramachandra Prasad, O. Anwar Bég, S. Kuharat, and T. A. Bég. "Magneto-Thermo-Gravitational Rayleigh–Bénard Convection of an Electro-Conductive Micropolar Fluid in a Square Enclosure: Finite Volume Computation." *Numerical Heat Transfer, Part A: Applications*, 2024, pp. 1–26. 10.1080/10407782.2023.2299290.
- XXVII. Venkatadri, K., Fazuruddin, S., O. Anwar Bég, and O. Ramesh. "Natural Convection of Nanofluid Flow in a Porous Medium in a Right-Angle Trapezoidal Enclosure: A Tiwari and Das' Nanofluid Model." *Journal of Taibah University for Science*, vol. 17, no. 1, 2023. 10.1080/16583655.2023.2263224.
- XXVIII. Venkatadri, K., K. V. Narasimha Murthy, T. A. Bég, O. Anwar Bég, and S. Kuharat. "Numerical Simulation of Natural Convection in a Rectangular Enclosure Filled with Porous Medium Saturated with Magnetic Nanofluid Using Buongiorno's Two-Component Model." *Canadian Journal of Chemical Engineering*, 2024, pp. 1–22. 10.1002/cjce.25300.

- XXIX. Venkatadri, K., T. S. Devi, A. Shobha, K. R. Sekhar, and V. R. Rajeswari. "Numerical Study of Natural Convection Flow in a Square Porous Enclosure Filled with Casson Viscoelastic Fluid." *Contemporary Mathematics*, vol. 4, no. 3, 2023, pp. 379–391. https://ojs.wiserpub.com/index.php/CM/article/view/2913.
- XXX. Vedavathi, N., K. S. Mozhi, K. Venkatadri, et al. "Numerical Analysis of Cu–H2O Nanofluid Natural Convection in a Trapezoidal Enclosure Filled with Porous Medium." *International Journal of Applied and Computational Mathematics*, vol. 9, 2023, p. 121. 10.1007/s40819-023-01602-7.